Observer based junction temperature estimation: 3D simulations and experimentations

Tychique Nzalalemba Kabwangala, Jean-Pierre Fradin, Yassine Ariba, Alexandre Marie, Frédéric Gouaisbaut

Observer based junction temperature estimation : 3D simulations and experimentations

1st Tychique Nzalalemba Kabwangala
LAAS-CNRS, Faculté d'ingénierie ULC-Icam
Université Loyola du Congo
Kinshasa, D.R. Congo
tychique.nzalalemba@ulc-icam.com

2nd Jean-Pierre Fradin
Toulouse campus
Icam School of Engineering
Toulouse, France
jean-pierre.fradin@icam.fr

3rd Yassine Ariba
LAAS-CNRS, INSA Toulouse
Université de Toulouse
Toulouse, France
yariba@laas.fr

4th Alexandre Marie
Toulouse campus
Icam School of Engineering
Toulouse, France
alexandre.marie@icam.fr

5th Frédéric Gouaisbaut
LAAS-CNRS, Université Paul Sabatier
Université de Toulouse
Toulouse, France
fgouaisb@laas.fr

***Abstract*—In this paper, a state-space modelling of power module with thermal sensors is proposed. This model is built from an identification method based on experimental and 3D simulation ($6SigmaET$) data. The purpose is to use automatic control theory to estimate the semiconductor junction temperature. Hence, a Luenberger full state observer is implemented to estimate the junction temperature. Such an algorithm uses the available measurements to adjust in real-time the junction temperature estimation. the results were confirmed with an experimental bench test.**

***Index Terms*—semiconductor, junction temperature monitoring, estimation, observer, automatic control**

I. Introduction

With the evolution of technologies that lead to the use of electronic components at high temperatures, the knowledge of the junction temperature is crucial since it prevents the semiconductor from overheating. The general purpose is to enable the thermal management of electronic power modules so as to increase their reliability and optimize their use with respect to large heat dissipation per unit area.

Several researches are currently mature for measuring a semiconductor chip temperature using thermal methods. They can be splitted into two categories: optical and physical contact methods. The first group utilizes infared cameras [1], thermo optic [2], photoluminence, reflectance, raman effects [3], etc. The second group uses thermocouples [4], thermistors [5], fiber optic [6], liquid cristal [6], [7], etc. But most of those methods are intrusive, i.e they require partial or total access to the power module in order to measure the temperature. This is a drawback for practical use where more and more power modules are cooled by fluids and cannot be opened during functioning. In addition, most of those measurements do not correspond to the actual chip junction temperature.

Other methods for junction temperature measurement are electrical ones. They use semiconductor thermosensitive electrical parameters (TSEP) [8], [9] to evaluate the temperature from an electrical measurement.These methods are non intrusive and are usually used for encapsulated semiconductors. However, most of these techniques are not suitable for industrial purposes since they require a controlled environment for a correct approximation of the junction temperature.

Several studies focus on estimating the temperature of semiconductors via analytical models [10]–[14]. Most of them are based on the equivalence to RC networks. Others use 3D thermal models [13], [14] based on finite difference or finite element methods.

In this paper, we use a mathematical model and correct the results with measurements. The authors of [15] used a similar mathematical approach by performing state representation identification methods with help of the system identification (SID) toolbox from MATLAB to compute the surface temperature in a machine tool application. However, most of the published researches are limited to retrieving the junction temperature via an identified system. These methods are not robust since they are open-loop calculations resulting directly from a model and are very sensitive to system disturbances [21]–[23].

Our contribution proposes an original approach which aims at retrieving the junction temperature of a semiconductor chip through thermal sensors using an observer algorithm methodology, from automatic control theory [24]–[26]. The contribution of this study relies on the design of a virtual sensor to estimate the junction temperature with a closed-loop structure. This approach is more robust to system disturbances.

II. System presentation and experimental setup

The power module studied in this paper is composed of 3 IGBT and 3 diodes assembled to a direct bonded copper (DBC) Curamik substrate. This module is instrumented with thermal sensors as illustrated in Fig.1. Only one diode (diode HS3) was powered during the experiments. The sensor data come from type K thermocouples. T_{ck4} and T_{ck5} are placed

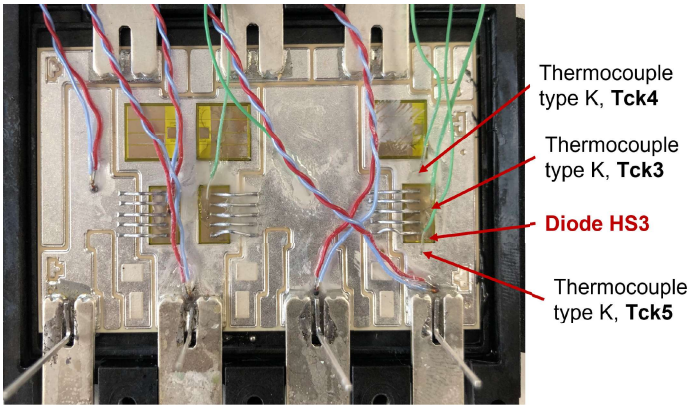

Fig. 1. Power module and thermocouples T_{ck3}, T_{ck4} and T_{ck5}. All three type K thermocouples are set up with cyanoacrylate glue.

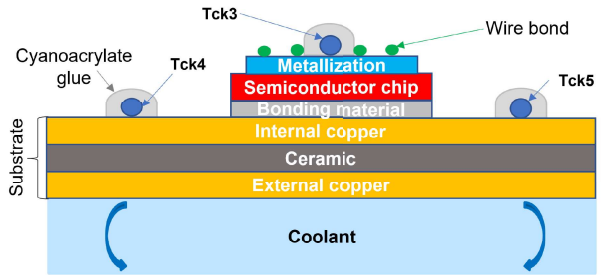

Fig. 2. Active diode 2D view and thermocouples placement.

in the neighbourhood of the active chip, on the substrate. T_{ck3} is placed on the active diode.

Fig.2 illustrates the structure of the power module in the diode HS3 transverse cross section. The associated materials properties are presented in Table I.

A. Test bench

The power module cooling is composed of 50/50 glycol water. The liquid temperature is maintained at $20°C$ using a thermocryostat. The test bench control is combined with a LabVIEW [16] program and a National Instruments acquisition system. The test bench used was designed for measuring thermal impedances with the pulsed heating curve technique. Thermocouples measurements are collected with the acquisition card PXIe-6345, incorporating a cold junction temperature compensation. The data are directly retrieved from the test bench via a LabVIEW interface.

B. Junction temperature measurement

The junction temperature measurement T_j on the test bench is performed using the diode on-state voltage under a measurement current of $10mA$. Indeed, under a low control voltage (some millivolts), the diode on-state voltage is temperature sensitive enough to be used as a TSEP that can provide information on the junction temperature.

C. 3D thermal numerical model

Since the test bench is limited to junction temperature measurements for step responses, a 3D thermal model has been designed with $6SigmaET$ software [17], [22] to extend the tests capability and have more flexibility in diode HS3 heating scenarios. The 3D thermofluidic model is composed of the power module CAD model, in which were added thermocouples CAD and boundary conditions such as 4 liters per minute (LPM) coolant flow rate and 69W dissipated power in diode HS3.

Thermocouples type K were modeled in the power module 3D thermal model in $6SigmaET$ software as illustrated in Fig.3. They are made of two separate wires soldered at the bottom. Since they are set on the power module with a cyanoacrylate glue, there is a $60 - 100\mu m$ gap between the soldered junction of the sensor wires and the power module components, depending on the thermocouple, in order to avoid measurement electrical perturbations. Power module components properties are presented in Table II.

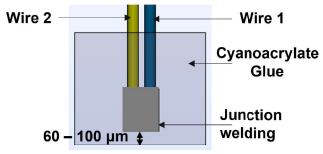

Fig. 3. Thermocouple type K numerical model in the thermofluidic simulation software $6SigmaET$.

In this paper, the junction temperature is defined as the average volumetric temperature of the active chip dissipation zone. Fig.4 shows the 3D thermofluidic model results after a 100 seconds of 69W step heating power in diode HS3.

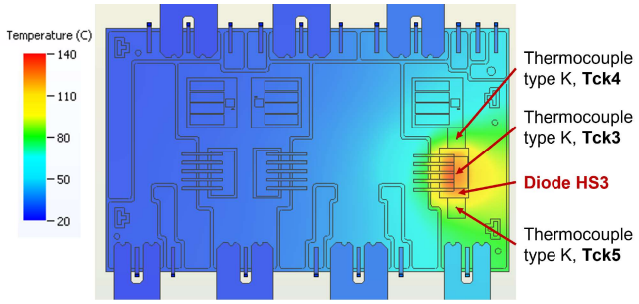

Fig. 4. Surface temperature temperature field computed by the 3D thermofluidic model after 100 seconds of 69W heat disspation on the active diode

Fig.5 shows that the 3D thermofluidic simulation model matches well the experimental results. $T_j - 69W\_Exp$ is the diode HS3 junction temperature curve coming from experimental data with a 69W dissipated step power. $T_j - 69W\_Simu$ is the the diode HS3 junction temperature response to 69W input step power obtained from the 3D thermal model developped in $6SigmaET$. T_{cki}_Exp and T_{cki}_Simu are the responses of thermocouples surrounding the active diode from respectively experiment and $6SigmaET$; with $i = 3, 4$ *or* 5. Differences between curves can be explained by the actual cyanoacrylate glue thickness and the thermocouple junction welding properties which are difficult to estimate. Especially, in steady state, $T_j - 69W\_Exp$ is almost the

TABLE I
POWER MODULE - PROPERTIES.

Component	Material	Density (Kg/m^3)	Cp ($J/Kg.K$)	Conductivity ($W/m.K$)
Wire bond	Aluminium	2700	921	235
Metallization	Aluminium	2700	921	235
Diode	Silicon	2330	700	Temperature dependent
Bonding material	Silver	10500	232	100
Internal copper	Copper	8950	380	386
ceramic	Alumina (DBC Curamik)	3985	900	24
External copper	Copper	8950	380	386
Coolant	50/50 glycol water	1073	3310	0.39

TABLE II
THERMOCOUPLE TYPE K - PROPERTIES.

Component	Material	Density (Kg/m^3)	Cp ($J/Kg.K$)	Conductivity ($W/m.K$)
Wire 1	Chromel	8500	447	18.4
Wire 2	Alumel	8600	489	30.6
Junction welding	Mixture of chromel-Alumel	8550	468	24.5
Glue	Cyanoacrylate	1070	1420	0.3

same as T_{ck3}_Exp and $T_j - 69W\_Simu$ is 4% lower than T_{ck3}_Simu.

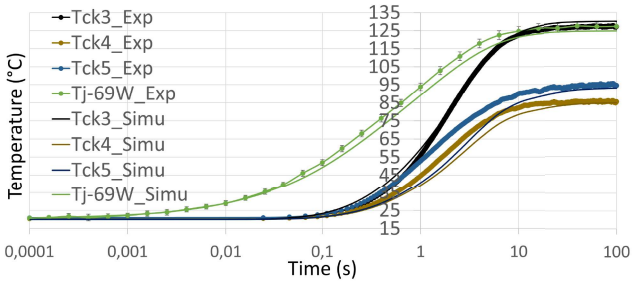

Fig. 5. Comparison between experimental and simulation data obtained with $6SigmaET$. Both junction temperature T_j and type K thermocouple measurements T_{ck3}, T_{ck4} and T_{ck5} are presented. See Fig.1 and Fig.4 for thermocouples locations.

Given the experimental data, an identification model can now be built with SID toolbox of MATLAB in order to develop a junction temperature observer.

III. SYSTEM IDENTIFICATION

Let us first define the system to be modeled and its inputs/outputs. It is assumed that there is a causality relationship between the junction temperature and the sensors measurements. Hence, we consider the power module with thermal sensors to be represented as in Fig.6. Two different 69W power signals are used for identification: step and pseudorandom binary sequence (PRBS) [18] signals. The first one is used to identify both subsystems with experimental data. While the second signal is applied for the identification with data from the thermofluidic 3D model implemented on $6SigmaET$ software. N4SID algorithms were employed in SID toolbox [15], [19], [20], using 6 state variables for each subsystem. The SID results lead to a state-space representation as follows:

$$\begin{cases} x(k+1) = A_i x(k) + B_i u(k) + K_i e_i(k) \\ y(k) = C_i x(k) + D_i u(k) + e_i(k) \end{cases} \quad (1)$$

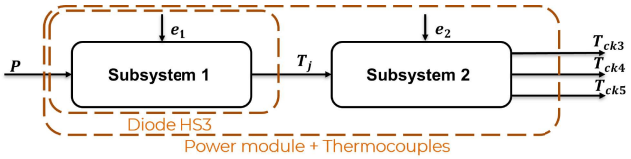

Fig. 6. Power module transfer function representation. For the subsystem 1, the power P is the input and the junction temperature T_j the output. For the subsystem 2, the junction temperature is considered as the input and T_{ck3}, T_{ck4} and T_{ck5} are the outputs. e_1 and e_2 represent some disturbances.

A_i : state matrix; B_i : control matrix; C_i : output matrix; D_i : feedthrough matrix; K_i : disturbance matrix; x : state vector; y : output signal(s); u : input signal(s); e_i : disturbance signal which is the set of all signals that can impact on the junction temperature (coolant flow rate, noise measurements, etc.) different from the controlled input signal; k : number of samples; i : 1 or 2, depending on the subsystem.

The identification algorithms provide numerical values for all matrices $\{A_i, B_i, C_i, D_i, K_i\}$. The obtained model is superimposed to the experimental data. Fig.7 illustrates the results for the experimental data and Fig.8 for 3D thermofluidic simulation model developed in $6SigmaET$ software. The fit percentage was determined by the normalized root mean square estimation (NRMSE) of goodness between the plotted data. In our case, more than 99% of fit was observed when the identified outputs were compared to the measurements or $6SigmaET$ data.

From Fig.7 and Fig.8, we can conclude that subsystems 1 and 2 identifications provide excellent results for both experiment and 3D simulation ($6SigmaET$) data. Since the identified models are sensitive to system disturbances which can be measurement noise or any other input signal not taken into account during the identification process (changes in coolant properties, coolant flow rate, etc.), an observer has been designed. The key idea is to provide an estimation of T_j

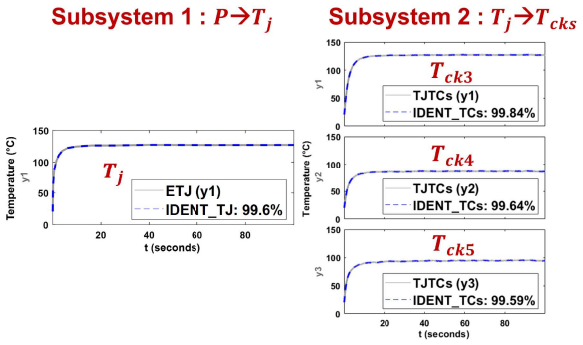

Fig. 7. Comparison between experiment data and identified subsystems outputs. The input signal is a 69W power step. The fit percentage is over 99% with 6 state variables.

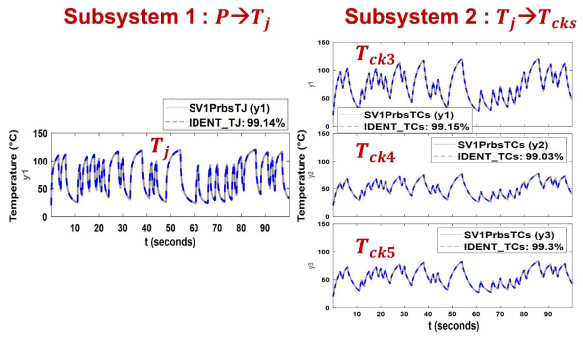

Fig. 8. Comparison between $6SigmaET$ data and identified subsystems outputs. The input power is a 69W PRBS signal. The fit percentage is over 99% with 6 state variables.

with closed-loop calculations to correct real-time mismatch.

IV. Observer Design

For the observer design, the state-space model representation is used without the disturbance signals as illustrated in Fig.9.

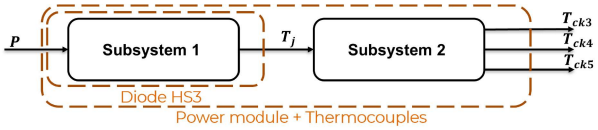

Fig. 9. Power module + thermal sensors transfer bloc representation without model disturbance.

We have then the following state-space representations:

$$\begin{cases} x_1(k+1) &= A_1x_1(k) + B_1P(k) \\ T_j(k) &= C_1x_1(k) + D_1P(k) \end{cases} \tag{2}$$

and

$$\begin{cases} & x_2(k+1) &= A_2x_2(k) + B_2T_j(k) \\ T_{cks}(k) &= \begin{bmatrix} T_{ck3}(k) \\ T_{ck4}(k) \\ T_{ck5}(k) \end{bmatrix} &= C_2x_2(k) + D_2T_j(k) \end{cases} \tag{3}$$

with

T_j : diode HS3 junction temperature; P: diode HS3 dissipated power; T_{cks}: Themocouples type K temperature measurements.

In the literature [10], [11], [13], [15], [21]–[23], current junction temperature estimation results are based on an open-loop model as presented in Fig.10. However, in our approach, a full state Luenberger observer is designed [24]–[26].

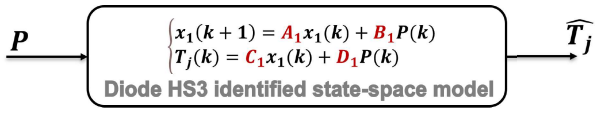

Fig. 10. Open-loop junction temperature estimation: identified model not corrected by thermal sensor measurements.

An observer is an algorithm that estimates an unmeasured variable. It uses the known input (the power P) and the available measurements T_{ck3}, T_{ck4} and T_{ck5} surrounding the active diode on the power module to estimate the unmeasured junction temperature T_j. This leads to a closed-loop model as presented in Fig.11. Basically, this real-time algorithm acts as a virtual sensor which is able to estimate the junction temperature T_j based on the measurements T_{cks}.

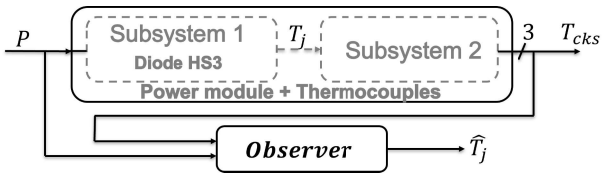

Fig. 11. Closed-loop junction temperature estimation representation: observer design using diode HS3 dissipated power and sensors temperature measurements.

Let consider subsystems (2) and (3) and $x = \begin{bmatrix} x_1 & x_2 \end{bmatrix}^T$ the extended state of the whole system. Replacing $T_j(k)$ by $C_1x_1(k) + D_1P(k)$, we get :

$$x_2(k+1) = B_2C_1x_1(k) + A_2x_2(k) + B_2D_1P(k) \tag{4}$$

and

$$T_{cks}(k) = D_2C_1x_1(k) + C_2x_2(k) + D_2D_1P(k) \tag{5}$$

Then, the extended system is defined by:

$$\begin{cases} x(k+1) = \begin{bmatrix} A_1 & 0 \\ B_2C_1 & A_2 \end{bmatrix} \begin{bmatrix} x_1(k) \\ x_2(k) \end{bmatrix} + \begin{bmatrix} B_1 \\ B_2D_1 \end{bmatrix} P(k) \\ T_{cks}(k) = \begin{bmatrix} D_2C_1 & C_2 \end{bmatrix} \begin{bmatrix} x_1(k) \\ x_2(k) \end{bmatrix} + D_2D_1P(k) \end{cases} \tag{6}$$

Its dynamic can then be written as:

$$\begin{cases} x(k+1) = \tilde{A}x(k) + \tilde{B}P(k) \\ T_{cks}(k) = \tilde{C}x(k) + \tilde{D}P(k) \end{cases} \tag{7}$$

with

$\tilde{A} = \begin{bmatrix} A_1 & 0 \\ B_2C_1 & A_2 \end{bmatrix}$; $\tilde{B} = \begin{bmatrix} B_1 \\ B_2D_1 \end{bmatrix}$;

$\tilde{C} = \begin{bmatrix} D_2C_1 & C_2 \end{bmatrix}$ and $\tilde{D} = D_2D_1$

The observer dynamic is composed of the aforementioned state space model plus a corrective term:

$$\begin{cases} \hat{x}(k+1) &= \tilde{A}\hat{x}(k) + \tilde{B}P(k) + G[T_j(k) - \hat{T}_j(k)] \\ \hat{T}_j(k) &= C_1\hat{x}_1(k) + D_1P(k) \end{cases} \tag{8}$$

where $\hat{x} = \begin{bmatrix}\hat{x}_1 & \hat{x}_2\end{bmatrix}^T$ is the internal state of the observer and corresponds to an estimation of x.

Basically, the observer is a model of the original system which dynamics are connected by the injection of the estimation error $T_j(k) - \hat{T}_j(k)$. The objective of the observer is then to reconstruct the entire state $x(k)$ and, especially, $T_j(k)$ for which the estimation is $\hat{T}_j(k) = \tilde{C}_1\hat{x}(k) + \tilde{D}_1P(k)$. Introducing the estimation error $e(k)$ between $x(k)$ and $\hat{x}(k)$, namely:

$$e(k) = x(k) - \hat{x}(k) \tag{9}$$

One obtains its dynamics:

$$e(k+1) = x(k+1) - \hat{x}(k+1) \tag{10}$$

$$\begin{aligned} e(k+1) = \quad & \tilde{A}x(k) + \tilde{B}P(k) - [\tilde{A}\hat{x}(k) + \tilde{B}P(k) \\ & + G(T_j(k) - \hat{T}_j(k))] \end{aligned} \tag{11}$$

$$e(k+1) = \tilde{A}[x(k) - \hat{x}(k)] - GC_1[x_1(k) - \hat{x}_1(k)] \tag{12}$$

$$e(k+1) = \tilde{A}[x(k) - \hat{x}(k)] - G\tilde{C}_1[x(k) - \hat{x}(k)] \tag{13}$$

$$e(k+1) = (\tilde{A} - G\tilde{C}_1)e(k) \tag{14}$$

or

$$e(k+1) = Fe(k) \tag{15}$$

where:

- $\tilde{C}_1 = \begin{bmatrix}C_1 & 0\end{bmatrix}$ and $F = \tilde{A} - G\tilde{C}_1$
- G is the observer gain to be designed

Then it is required to compute G such that $e(k)$ converges to zero faster than the dominant dynamic of the overall system. It means that G have to be designed such that the eigenvalues of F have a modulus strictly less than one. According to the Kalman rank condition [26], this is always possible if the pair $(\tilde{A},\tilde{C})$ is observable, that is $Rank\begin{bmatrix}\tilde{C}^T & (\tilde{C}\tilde{A})^T & \dots & (\tilde{C}\tilde{A}^{n-1})^T\end{bmatrix}^T = n$ where n is the dimension of the extended state-space.

In our study, for the matrices obtained in the models (2) and (3), this latter condition is satisfied.

V. Results and Discussion

In this section, experimental tests have been carried out with our test bench. For different scenarios, we will compare results of the temperature estimation with the observer (8) (see Fig.11, closed loop approach) and the classical prediction with simply the model of the process (2) (see Fig.10, open-loop approach).

Fig.12 shows a scenario where the identified model with null states initial conditions and an input 55W power is compared to the experimental measurement at the same dissipated power. The static error between both curves is due to TSEP lower sensibility to the current in lower powers and the impact of measurement disturbance. Then, the identified model is less accurate. However, in the closed-loop configuration, the observer built from experimental data set takes into account the sensor measurements to adjust the static error. Thus, a much better junction temperature estimation is obtained with the observer algorithm. Note that the great gap observed before the first second in the closed-loop configuration is due to observer initial conditions which are far from the real ones and the convergence speed imposed by the observer gain.

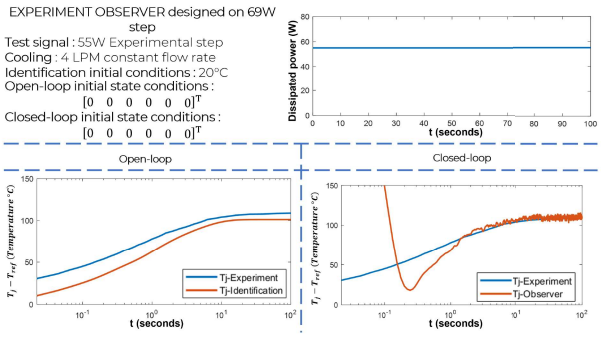

Fig. 12. Open-loop VS closed-loop junction temperature estimation: experiment data observer designed based on 69W step power and tested with 55W step power having a 4 LPM constant cooling flow rate.

In Fig.13 and Fig.14, a change in the cooling flow rate has been introduced to simulate some default in the power module cooling system. Such changes were not taken into account in the identified model which only depends on the dissipated input power. As a result, the junction temperature response with the open-loop prediction model cannot capture the junction temperature change induced by flow rate variations. However, the observer algorithm can manage some corrections to the junction temperature estimation whenever the sensors record any change in temperature T_{ckl}. In Fig.13, the observer is built from experiment data set and the test signal is from the 3D thermal model.

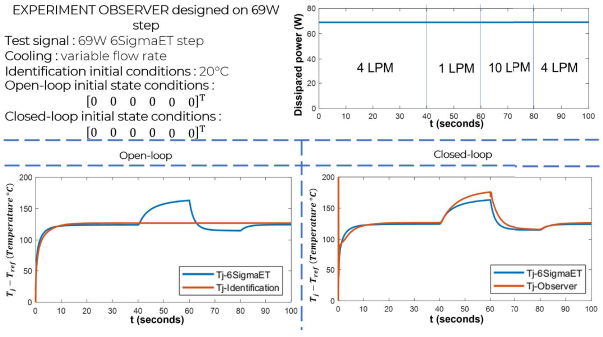

Fig. 13. Open-loop VS closed-loop junction temperature estimation: experiment data observer designed based on 69W step power and tested with 69W step power and a variable cooling flow rate.

In Fig.14, the observer is built from 3D thermal model data set and the test signal is also from the simulated $6SigmaET$ model. Note that, when an abrupt change is noticed in the system, some spikes may come up in the estimate $\hat{T}_j$, which amplitudes depend on the observer gain. Those spikes can be

reduced by taking into account disturbance rejection criterion in the design of the observer gain.

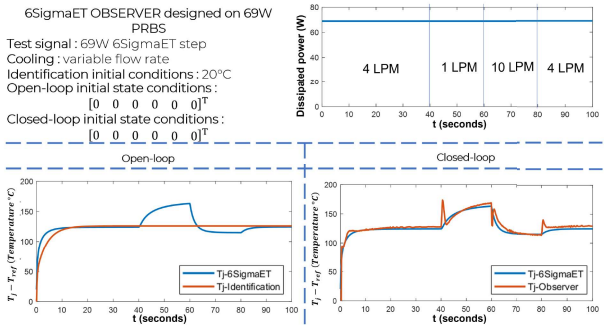

Fig. 14. Open-loop VS closed-loop junction temperature estimation: 3D simulation data observer designed based on 69W PRBS power and tested with 69W step power and a variable cooling flow rate.

It is noticed that the thermal flow path tends to change with the flow rate. This have an impact on the observer results since the identified model from which it is built will no longer be valid.

VI. Conclusion

A six chips power module where only one diode is active and instrumented with three type K thermocouples in its neighborhood has been modelled by a state-space approach. The overall system was identified via MATLAB SID toolbox using experimental and 3D thermal model data sets. Consecutively to the verification of the Kalman observability criterion on the identified system, it was possible to design an observer which is able to reconstruct the diode junction temperature with regards of the thermal sensors measurements corrections. This closed-loop approach is better then the open-loop one widely used in the literature. Simulation and experimental tests have validated the proposed methodology. These original and promising results can be improved in future works with robust control techniques, adaptive filter techniques or artificial intelligence to design an observer gain yielding to better performance properties (responsiveness, overshoot) and reduced sensitivity to noise or uncontrolled disturbances.

References

[1] L. Dupont, Y. Avenas, and P.-O. Jeannin, "Comparison of junction temperature evaluations in a power IGBT module using an IR camera and three thermosensitive electrical parameters," IEEE Transactions on Industry Applications, vol. 49, no 4, p. 1599-1608, 2013.

[2] C. C. Lee, T. J. Su and Mingcher Chao, "Transient thermal measurements using thermooptic and thermoelectric effects," 8th Annual IEEE Semiconductor Thermal Measurement and Management Symposium, 1992, pp. 41-46.

[3] M. Kuball et al., "Time-Resolved Temperature Measurement of AlGaN/GaN Electronic Devices Using Micro-Raman Spectroscopy," in IEEE Electron Device Letters, vol. 28, no. 2, pp. 86-89, 2007.

[4] B. Du, J. L. Hudgins, E. Santi, A. T. Bryant, P. R. Palmer and H. A. Mantooth, "Transient Electrothermal Simulation of Power Semiconductor Devices," in IEEE Transactions on Power Electronics, vol. 25, no. 1, pp. 237-248, 2010.

[5] M. Shawky, "Using Thermistors to Optimize the Thermal Performance of IGBT Modules," Texas Instruments, Temperature and Humidity Sensing, p. 3, 2019.

[6] J. F. Algorri, B. García-Cámara, A. García-García, V. Urruchi and J. M. Sánchez-Pena, "Fiber Optic Temperature Sensor Based on Amplitude Modulation of Metallic and Semiconductor Nanoparticles in a Liquid Crystal Mixture," in Journal of Lightwave Technology, vol. 33, no. 12, pp. 2451-2455, 2015.

[7] K. Azar and D. J. Farina, "Measuring chip temperature with thermochromic liquid crystals," Electronics Cooling, vol. 3, p. 16-22, 1997.

[8] A. Griffo, J. Wang, K. Colombage and T. Kamel, "Real-Time Measurement of Temperature Sensitive Electrical Parameters in SiC Power MOSFETs," in IEEE Transactions on Industrial Electronics, vol. 65, no. 3, pp. 2663-2671, 2018.

[9] Y. Avenas, L. Dupont and Z. Khatir, "Temperature Measurement of Power Semiconductor Devices by Thermo-Sensitive Electrical Parameters—A Review," in IEEE Transactions on Power Electronics, vol. 27, no. 6, pp. 3081-3092, 2012.

[10] Z. Luo, H. Ahn and M. A. E. Nokali, "A thermal model for insulated gate bipolar transistor module," in IEEE Transactions on Power Electronics, vol. 19, no. 4, pp. 902-907, 2004.

[11] A. Ammous, S. Ghedira, B. Allard, H. Morel and D. Renault, "Choosing a thermal model for electrothermal simulation of power semiconductor devices," in IEEE Transactions on Power Electronics, vol. 14, no. 2, pp. 300-307, 1999.

[12] G. L. Skibinski and W. A. Sethares, "Thermal parameter estimation using recursive identification," in IEEE Transactions on Power Electronics, vol. 6, no. 2, pp. 228-239, 1991.

[13] A. Cassou, Q. C. Nguyen, P. Tounsi, J.-P. Fradin, M. Budinger, and I. Hazyuk, "Extraction of compact transient thermal models for a global optimization of a power system based on SiC MOSFETs switches," 26th International Workshop on Thermal Investigations of ICs and Systems (THERMINIC), 2020. hal-03655834.

[14] S. Dutta, B. Parkhideh, S. Bhattacharya, G. K. Moghaddam and R. Gould, "Development of a predictive observer thermal model for power semiconductor devices for overload monitoring in high power high frequency converters," 27th Annual IEEE Applied Power Electronics Conference and Exposition (APEC), 2012, pp. 2305-2310.

[15] Y.-C. Hu, P.-J. Chen and P.-Z. Chang, "Thermal-Feature System Identification for a Machine Tool Spindle," Sensors, 2019; 19(5):1209.

[16] J. Travis and J. Kring, "LabVIEW for everyone : graphical programming made easy and fun," 3rd edition, Upper Saddle River, NJ: Prentice Hall, 2006. ISBN 0131856723.

[17] A. Fodor, A. Taut and G. Chindris, "Increasing Thermal Simulation Efficiency with 6SigmaET," 2021 IEEE 27th International Symposium for Design and Technology in Electronic Packaging (SIITME), 2021, pp. 41-44.

[18] J. Schoukens, K. Godfrey and M. Schoukens, "Nonparametric Data-Driven Modeling of Linear Systems: Estimating the Frequency Response and Impulse Response Function," in IEEE Control Systems Magazine, vol. 38, no. 4, pp. 49-88, 2018.

[19] T. W. Flint and R. J. Vaccaro, "Performance analysis of N4SID state-space system identification," Proceedings of the ACC (IEEE Cat. No.98CH36207), 1998, pp. 2766-2767 vol.5.

[20] T. J. A. Eguia, R. Shen, S. X. D. Tan, E. H. Pacheco and M. Tirumala, "Architecture level thermal modeling for multi-core systems using subspace system method," 2009 IEEE 8th International Conference on ASIC, 2009, pp. 714-717.

[21] Y. Yu, T. T. Lee and V. A. Chiriac, "Compact Thermal Resistor-Capacitor-Network Approach to Predicting Transient Junction Temperatures of a Power Amplifier Module," in IEEE Transactions on Components, Packaging and Manufacturing Technology, vol. 2, no. 7, pp. 1172-1181, 2012.

[22] A. Cassou, P. Tounsi and J. Fradin, "Compact thermal modelling for fast simulating consequences of pump defect: application to power module with double efficient cooling," 24rd International Workshop on Thermal Investigations of ICs and Systems (THERMINIC), 2018, pp. 1-5.

[23] J.-K. Kim, W. Nakayama, Y. Ito, S.-m. Shin and S.-K. Lee, "Estimation of thermal parameters of the enclosed electronic package system by using dynamic thermal response," Mechatronics, Volume 19, Issue 6, 2009, Pages 1034-1040, ISSN 0957-4158.

[24] D. Luenberger, "An introduction to observers," in IEEE Transactions on Automatic Control, vol. 16, no. 6, pp. 596-602, December 1971.

[25] G. Ellis,"Observers in Control Systems," Academic Press, 2002, Pages 1-259, ISBN 9780122374722.

[26] L. C. Westphal,"Handbook of Control Systems Engineering," Netherlands, Springer US, 2001, pp 253-694.